RSC Advances

PAPER

View Article Online
View Journal | View Issue

Cite this: RSC Adv., 2018, 8, 7055

Comparing the role of annealing on the transport properties of polymorphous $AgBiSe_2$ and monophase $AgSbSe_2$†

Minmin Zou, *[a] Qing Liu,[ab] Chao-Feng Wu,[c] Tian-Ran Wei,[c] Qing Tan,[d] Jing-Feng Li [c] and Fei Chen[a]

Received 27th November 2017
Accepted 5th February 2018

DOI: 10.1039/c7ra12819c

rsc.li/rsc-advances

$AgBiSe_2$ and $AgSbSe_2$, two typical examples of Te-free I–V–VI_2 chalcogenides, are drawing much attention due to their promising thermoelectric performance. Both compounds were synthesized *via* melting and consolidated by spark plasma sintering. The role of annealing on the transport properties of polymorphous $AgBiSe_2$ and monophase $AgSbSe_2$ was studied. Annealing has a greater impact on $AgBiSe_2$ than $AgSbSe_2$, which is ascribed to the temperature dependent phase transition of $AgBiSe_2$. Unannealed $AgBiSe_2$ shows p–n switching, but annealed $AgBiSe_2$ exhibits n-type semiconducting behavior over the whole measurement temperature range. By performing high-temperature Hall measurements, we attribute this intriguing variation to the change in the amount of Ag vacancies and mid-temperature rhombohedral phase after annealing. Both $AgBiSe_2$ and $AgSbSe_2$ exhibit low thermal conductivity values, which are ~0.40–0.50 W m^{-1} K^{-1} for $AgSbSe_2$ and ~0.45–0.70 W m^{-1} K^{-1} for $AgBiSe_2$, respectively. The maximum *ZT* value of $AgBiSe_2$ is enhanced from 0.18 to 0.21 after annealing. Pristine $AgSbSe_2$ presents a *ZT* value as high as 0.60 at 623 K, although slight deterioration emerges after annealing.

Introduction

Nowadays the demand for replaceable clean energy is becoming urgent due to the shortage of non-renewable fossil fuels and ever-increasing serious environmental pollution. Thermoelectric materials, capable of converting waste heat to electrical energy, have received extensive interest.[1–6] The energy conversion efficiency of a thermoelectric device is dependent on the dimensionless figure of merit (*ZT*) of the component materials. *ZT* is generally defined as $ZT = \alpha^2T/\rho\kappa$, where T is the absolute temperature, α is the Seebeck coefficient, ρ is the electrical resistivity, and κ is the thermal conductivity.

There are two feasible strategies to attain high *ZT* values. One is improving power factor (α^2/ρ) by carrier optimization and band engineering,[7,8] the other is reducing thermal conductivity by all-scale hierarchy design.[9–11] In recent years, complex nanostructures were designed; nanoscale precipitates, second phase particles as well as nano dots were introduced in bulk materials. However, it is challenging to controllably and reproducibly prepare such materials with reduced dimensions. Besides, nanostructures may grow or dissolve during prolonged high temperature operation. Therefore, thermoelectric materials with intrinsically low thermal conductivity are particularly appealing, among which I–V–VI_2 compounds (where I = Cu, Ag or alkali metal; V = Sb, Bi; and VI = S, Se, Te) emerge as new candidates.[12–21] The intrinsically low lattice thermal conductivity (κ_l) of I–V–VI_2 compounds arises from the strong lattice anharmonicity that is believed to associate with the lone pair electrons (s electrons) on the group V atoms.[22–24] Among numerous I–V–VI_2 compounds, $AgSbTe_2$ is widely studied due to the low thermal conductivity and high Seebeck coefficient. $AgSbTe_2$ alloys with GeTe (TAGS)[25–27] and PbTe (LAST-m),[28] are well known for their remarkable *ZT* values. However, the thermodynamic instability and the rarity of Te element hindered the development of $AgSbTe_2$-based thermoelectric materials.

$AgBiSe_2$ and $AgSbSe_2$, as homologues of $AgSbTe_2$, in which relatively less expensive and earth-abundant element Se is used to replace Te, seem to be more attractive. $AgBiSe_2$ exhibits an intriguing temperature dependent phase transition behavior,[12,13,15,29,30] which crystallizes in a hexagonal phase (space group $P\bar{3}m1$, α phase) at room temperature. As temperature increases, $AgBiSe_2$ undergoes a phase transition to rhombohedral phase (space group $R\bar{3}m$, β phase) at ~470 K and then to face-centered cubic phase (space group $Fm\bar{3}m$, γ phase)

[a]School of Materials Science and Engineering, Beijing Institute of Petrochemical Technology, Beijing, 102617, China. E-mail: zouminmin@bipt.edu.cn
[b]College of Materials Science and Engineering, Beijing University of Chemical Technology, Beijing 100029, China
[c]State Key Laboratory of New Ceramics and Fine Processing, School of Materials Science and Engineering, Tsinghua University, Beijing, 100084, China
[d]State Key Laboratory for Advanced Metals and Materials, University of Science and Technology Beijing, Beijing 100083, China

† Electronic supplementary information (ESI) available. See DOI: 10.1039/c7ra12819c

with disordered Ag and Bi positions at ∼580 K. In contrast, $AgSbSe_2$ crystallizes in a cubic phase in the whole temperature range. Colloidal method has been adopted to prepare I–V–VI_2 compounds, and high *ZT* values over unity were achieved in both pristine $AgBiSe_2$ (ref. 13) and $AgBi_{0.5}Sb_{0.5}Se_2$-based solid-solutioned homojunction nanoplates.[31] Meanwhile, remarkable enhancement of thermoelectric performance was observed in solid-state route synthesized I–V–VI_2 compounds through element doping, such as Nb/In doping[13,14] at Ag site and anion (Cl/Br/I) doping[29] at Se site in $AgBiSe_2$, Pb/Bi/Cd/Na/Mg/Ba doping[14,32–34] at Sb site and Sn doping[35] at Se site in $AgSbSe_2$, *etc.* To our surprise, $AgBiSe_2$ synthesized by solution method is a p-type semiconductor at ambient temperature, and reversible p–n–p conduction type switching is also observed in as-prepared $AgBiSe_2$.[13,31] However, the Seebeck coefficient values of $AgBiSe_2$ prepared *via* solid-state route indicate that $AgBiSe_2$ is n-type semiconductor.[15–17,29] Thus, the intrinsic transport behavior of $AgBiSe_2$ is still an open issue worth further exploration.

It is well known that annealing treatment is a common method used to eliminate defects and to improve the uniformity of microstructure and distribution of composition. The thermoelectric performance will be stable after annealing and transport properties of annealed samples should be close to the intrinsic value. Although long-term annealing has been applied to LAST compounds,[36,37] to our knowledge, the effect of annealing on polymorphous $AgBiSe_2$ and monophase $AgSbSe_2$ has not been reported yet.

In this work, we report the synthesis and thermoelectric properties of undoped $AgBiSe_2$ and $AgSbSe_2$. To gain an insight into the intrinsic transport behavior, annealing treatment was applied to the SPS-ed bulk samples, and high-temperature Hall measurement was used to investigate the temperature dependent carrier concentration of $AgBiSe_2$. It is found that annealing has greater impact on polymorphous $AgBiSe_2$ than monophase $AgSbSe_2$, which is ascribed to the temperature dependent phase transition of $AgBiSe_2$. Unannealed $AgBiSe_2$ shows a p–n switching, but annealed $AgBiSe_2$ exhibits n-type semiconducting behavior in the whole temperature range. The *ZT* value of $AgBiSe_2$ is improved after annealing due to significant reduction in electrical resistivity, with a peak value of 0.21 at 673 K. $AgSbSe_2$ displays better thermoelectric performance, and a maximum *ZT* value of 0.60 is achieved at 623 K, which slightly declines after annealing.

Experimental

Ingots of $AgBiSe_2$ and $AgSbSe_2$ were prepared by mixing stoichiometric Ag (99.95%), Bi (99.999%), Sb (99.999%) and Se (99.99%) in quartz tubes. The tubes were flame sealed under a high vacuum (∼10^{-4} Torr) and slowly heated to 673 K by 12 h, and then heated up to 1123 K in 4 h, soaked for 10 h, and subsequently cooled to room temperature. The as-prepared ingots were hand milled into powders by agate mortar. The derived powders were sintered in vacuum using a spark plasma sintering (SPS) system (Sumitomo SPS1010) under an axial compressive stress of 50 MPa at 673 K for 5 min. In order to study the effect of annealing on the thermoelectric performance of $AgBiSe_2$ and $AgSbSe_2$, the as-sintered samples were annealed in vacuum tube furnace at 673 K for 12 h.

Structural investigations were carried out by X-ray diffractometry (XRD, Bruker D8 Advance, Germany) using Cu Kα radiation. Rietveld refinements were carried out using the GSAS II software.[38] The average crystal structure of the $AgBiSe_2$ was refined using the $P\bar{3}m1$ space group and a minority $R\bar{3}m$ phase of $AgBiSe_2$. Fit indicators: R_{wp}, R_{exp}, and χ^2 were used to assess the quality of the refined structural models. The microscopic morphology and chemical composition of all samples were studied by field emission scanning electron microscopy (FE-SEM, Carl Zeiss Merlin, Germany) with energy dispersive X-ray spectrometer (EDS). The compositions were also measured by inductive coupled plasma emission spectrometer (ICP, IRIS Intrepid II XSP). The Seebeck coefficient and electrical resistivity were measured simultaneously on a ZEM-2 instrument system (Ulvac-Riko, Japan). The thermal conductivity was determined *via* $\kappa = D \times C_p \times d$, where D is the thermal diffusivity, C_p is the heat capacity, and d is the density. The thermal diffusivity was derived from the laser flash method (TC-9000, Ulvac-Riko, Japan). The heat capacity was estimated using the Dulong–Petit law, and the obtained values ($C_p = 0.210$ J g^{-1} K^{-1} for $AgBiSe_2$ and $C_p = 0.257$ J g^{-1} K^{-1} for $AgSbSe_2$) were close to the measured results.[14,29] The density was measured by the Archimedes method. The Hall coefficients, R_H, of the samples were characterized using a Hall coefficient measurement system (Resi-DC8340, Toyo, Japan). The Hall carrier concentration (n_H) was calculated by $n_H = 1/eR_H$, where e is the electronic charge.

Results and discussion

Fig. 1 shows the XRD patterns of bulk $AgBiSe_2$ and $AgSbSe_2$ samples at different stage of preparation. $AgSbSe_2$ crystallized in a cubic phase (PDF#65-6604) after melting. No obvious variation in the diffraction patterns is observed in both the samples after SPS and after annealing, except for slight broadening of the peaks. $AgBiSe_2$ ingot crystallizes in a hexagonal phase (PDF#74-0842) after melting. The XRD patterns of $AgBiSe_2$ are broadened and the relative intensity of (110) and (108) peak changes both after SPS and after annealing, which may originate from poor crystallinity of the SPS-ed sample compared with the ingot, or from the residual stress after SPS, or from the mixed phase constituent after SPS. On the one hand, the cooling rate of SPS is so fast that the high temperature cubic phase has not changed to hexagonal phase completely, thus a significant portion of the sample is frozen in the mid-temperature rhombohedral phase at room temperature. On the other hand, the lattice parameters of hexagonal phase ($P\bar{3}m1$, $a = 4.194$ Å, $c = 19.65$ Å) and rhombohedral phase ($R\bar{3}m$, $a = 4.184$ Å, $c = 19.87$ Å) are extremely close to each other,[15] so it is hard to identify one from the other.

Rietveld refinements were conducted to calculate the exact percentage of rhombohedral phase in all the $AgBiSe_2$ samples. Fig. 2 shows the Rietveld refinement data of powder XRD patterns of $AgBiSe_2$ obtained after melting, SPS and annealing. It should be noted that the XRD patterns of powder $AgBiSe_2$ is slightly different from that of bulk $AgBiSe_2$ samples, especially

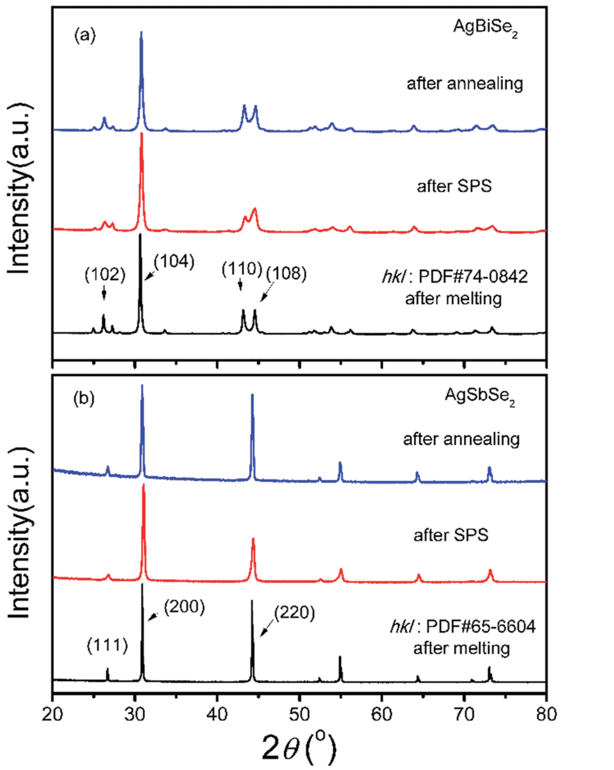

Fig. 1 XRD patterns of bulk samples after melting, SPS and annealing, (a) $AgBiSe_2$ and (b) $AgSbSe_2$.

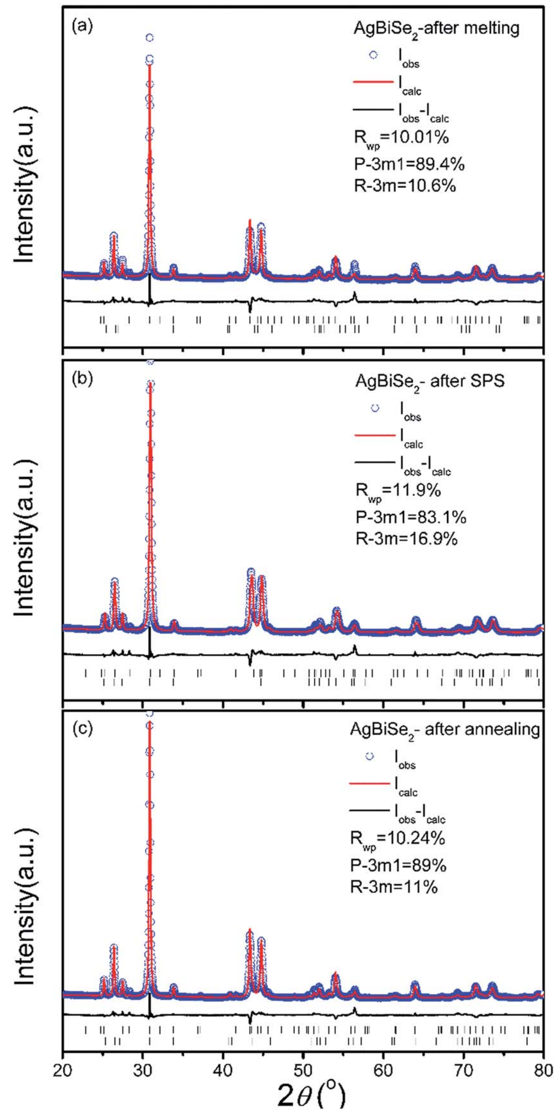

Fig. 2 Rietveld refinement of powder XRD patterns of $AgBiSe_2$ at different stage of preparation (a) after melting, (b) after SPS and (c) after annealing.

for the "after SPS" sample, which is mainly due to release of residual stress by grinding to powders. As shown in Fig. 2, the fractions of the rhombohedral phase are 10.6, 16.9 and 11%, respectively. The lattice parameters of $AgBiSe_2$ are listed in Table S1.† Similar phenomenon was also observed by Böcher *et al.*[17] It is reported that the fraction of the rhombohedral phase was ~11–16% in all the $Ag_{1-x}BiSe_2$ samples revealed by the Rietveld refinement of synchrotron diffraction data. Above discussion leads us to a conclusion that a small quantity of mid-temperature rhombohedral phase exists in all the $AgBiSe_2$ samples, and the proportion of rhombohedral phase decrease from 16.9% for unannealed $AgBiSe_2$ to 11% for annealed $AgBiSe_2$ due to the effect of annealing. Moreover, XRD patterns of bulk $AgBiSe_2$ samples with different annealing process are shown in Fig. S1.† Except the sample cooling by water quenching, other samples show almost identical XRD patterns.

The electrical resistivity of $AgBiSe_2$ and $AgSbSe_2$ prior to and after annealing is shown in Fig. 3(a). The resistivity of $AgBiSe_2$ declines drastically after annealing, from 5.1×10^4 μΩ m to 1.3×10^3 μΩ m at 323 K, which can be ascribed to either the reduction of defects after annealing or the mild change in phase constituent as discussed above about the XRD results. In contrast, the electrical resistivity of $AgSbSe_2$ increases after annealing, which may be attributed to the slight inevitable oxidation during the annealing process. The electrical resistivity of both annealed and unannealed $AgBiSe_2$ initially decreases with increasing temperature below 480 K, then increases in the temperature range of 480–580 K, showing a metallic transport behavior, and finally decreases again above ~580 K. Combining with the temperature dependent structural phase transition of $AgBiSe_2$, it is easy to conclude that 480 K and 580 K correspond to the α–β and β–γ phase transition temperature, respectively. The reduction of electrical resistivity in $AgBiSe_2$ above 580 K can be ascribed to the cubic phase crystallized at high temperature.

The Seebeck coefficient of $AgBiSe_2$ and $AgSbSe_2$ prior to and after annealing is shown in Fig. 3(b). The Seebeck coefficient of unannealed $AgBiSe_2$ changes from positive to negative with increasing temperature, indicating that the majority carrier varies from hole to electron. Such p–n switching is also found in solution synthesized $AgBiSe_2$,[13] while the only difference is that we did not observe further n–p switching during the β–γ phase transition. The Seebeck coefficient of $AgBiSe_2$ after annealing is negative in the entire temperature range, which suggests that electrons are the majority charge carrier in annealed $AgBiSe_2$. $|S|$ of $AgBiSe_2$ after annealing remains flat blow 480 K, then

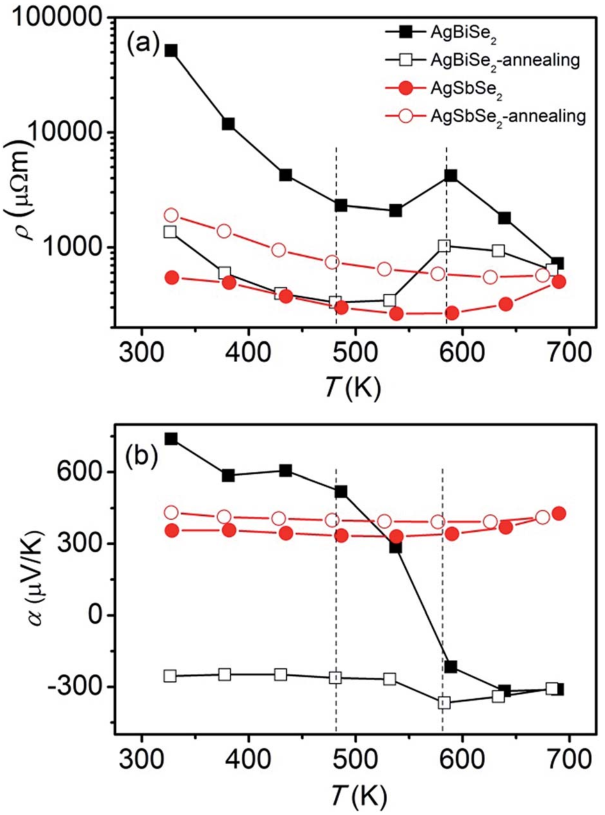

Fig. 3 Temperature dependent (a) electrical resistivity and (b) Seebeck coefficient of $AgBiSe_2$ and $AgSbSe_2$ prior to and after annealing. The two vertical dotted lines are only guides for eyes.

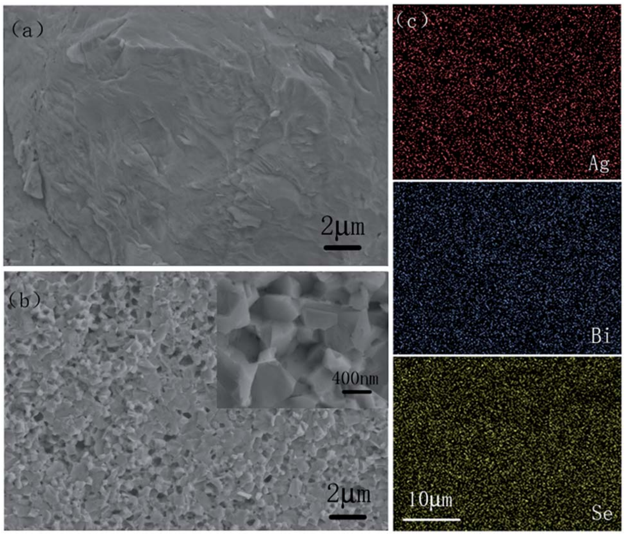

Fig. 4 SEM images of fracture surface for (a) unannealed $AgBiSe_2$ and (b) annealed $AgBiSe_2$; (c) EDS mapping for the elements Ag, Bi and Se of annealed $AgBiSe_2$. The inset picture in (b) is the high magnification image of annealed $AgBiSe_2$.

Table 1 Density and chemical composition of $AgBiSe_2$ prior to and after annealing

Samples	Density (g cm^{-3})	ICP atomic ratio Ag : Bi : Se
$AgBiSe_2$	7.89	25.08 : 25.28 : 49.64
$AgBiSe_2$-annealing	7.88	24.84 : 25.66 : 49.50

increases markedly with increasing temperature, reaching the maximum value at 580 K, and then starts to decrease finally. The positive Seebeck coefficient of $AgSbSe_2$ prior to and after annealing suggests that the carrier is dominated by hole in $AgSbSe_2$, which are 355 μV K^{-1} and 431 μV K^{-1} at 323 K for $AgSbSe_2$ before and after annealing, respectively. The relatively large Seebeck coefficient obtained in $AgSbSe_2$ is related to the flat valence band maximum and multi-peak valence band structure.[39]

Considering that the variation of composition may lead to the change of transport behavior of $AgBiSe_2$ after annealing, the microstructure and chemical composition of $AgBiSe_2$ prior to and after annealing were investigated. Typical morphologies of fresh fracture surfaces for $AgBiSe_2$ prior to and after annealing are exhibited in Fig. 4(a) and (b). It is interesting to find that the fracture model changes from predominantly transgranular fracture for unannealed $AgBiSe_2$ to intergranular fracture for annealed $AgBiSe_2$. The average grain size of annealed $AgBiSe_2$ is ~300–400 nm as displayed by the inset picture of Fig. 4(b). Elements of Ag, Bi and Se have a homogeneous distribution in annealed $AgBiSe_2$ sample as shown in Fig. 4(c). The density and ICP composition of $AgBiSe_2$ are listed in Table 1. Both samples have high density, which are 7.89 g cm^{-3} for unannealed $AgBiSe_2$ and 7.88 g cm^{-3} for annealed $AgBiSe_2$, corresponding to 98.6% and 98.5% of the theoretical density. Although the fracture surface of annealed $AgBiSe_2$ seems more porous, the density is nearly unchanged. Because the "holes" are just left by pulling out other crystal grains, not real pores, as shown in the inset picture of Fig. 4(b). The ICP atomic ratios of Ag : Bi : Se for unannealed $AgBiSe_2$ and annealed $AgBiSe_2$ are similar, and the ratio values are close to the nominal value. The slight deviation from stoichiometric ratio of Se in both samples may be attributed to the volatilization during fabrication process. Thus, it is supposed that the variation of composition is too small to influence the transport behavior of $AgBiSe_2$.

In order to clarify the extraordinary change in the Seebeck coefficient of $AgBiSe_2$, high-temperature Hall coefficient measurement was conducted. The temperature dependent Hall carrier concentration of $AgBiSe_2$ prior to and after annealing is plotted in Fig. 5. It should be noted that the sign of the carrier concentration is just used to represent the type of the majority carrier (negative for electron, positive for hole). What should also be declared is that the measurement uncertainty is about 5% for most temperature points, while the uncertainty could be 15–20% at 573 K, which might be ascribed to the undergoing β–γ phase transition at that temperature. Thus, the Hall carrier concentration at 573 K might be not so precise. Nevertheless, the trend of carrier concentration is still persuasive. Obviously, hole is the majority carrier below ~523 K in unannealed $AgBiSe_2$, but electron is predominant above ~523 K, which offers solid evidence for the p–n switching behavior. The

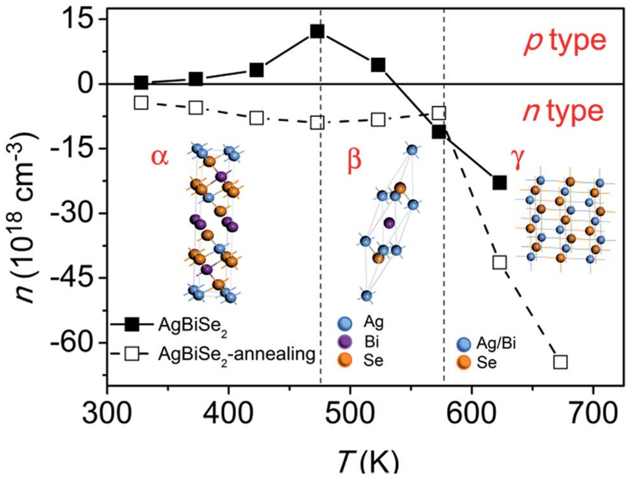

Fig. 5 Temperature dependent Hall carrier concentration of $AgBiSe_2$ prior to and after annealing. The two vertical dotted lines are only guides for eyes.

majority carrier of $AgBiSe_2$ changes from hole to electron after annealing, which is consistent with the tendency of Seebeck coefficient. Typically, the Hall carrier concentration changes from 1.34×10^{17} cm^{-3} (hole) for unannealed $AgBiSe_2$ to 3.74×10^{18} cm^{-3} (electron) for annealed $AgBiSe_2$ at 323 K. Similar electron concentration of 5.85×10^{18} cm^{-3} was obtained by Guin *et al.* in pristine $AgBiSe_2$.[29] Pan *et al.* also reported a high electron concentration of 1.5×10^{19} cm^{-3} in n-type $AgBiSe_2$.[15] Regardless of carrier type, the Hall carrier concentration of both samples increases with increasing temperature below ~480 K, then decreases in the rhombohedral phase temperature range, and finally increases above 580 K, displaying close connection with the temperature dependent phase transition of $AgBiSe_2$. Mid-temperature rhombohedral phase $AgBiSe_2$ is a semiconductor, whereas the high-temperature cubic phase with disordered arrangements of Ag and Bi atoms is found to be metallic.[30] Thereby, the electrical transport behavior exhibits a semiconducting to metallic transition when going from rhombohedral to cubic phase, leading to the remarkable enhancement of carrier concentration above 580 K. Based on the variation of carrier concentration, the trends of electrical resistivity and Seebeck coefficient of $AgBiSe_2$ can be well understood. Combining the results of electrical resistivity and Seebeck coefficient with carrier concentration, the possible reason for the distinct change of electrical transport behavior after annealing can be explained as following: (1) amount of defects exist in the SPS-ed $AgBiSe_2$ sample, such as Ag vacancies, which act as hole dopants in $AgBiSe_2$, leading to p-type transport behavior;[13] (2) the existence of mid-temperature rhombohedral phase may contributes to the high electrical resistivity of unannealed $AgBiSe_2$, for the rhombohedral phase has a higher electrical resistivity than the hexagonal phase;[16] (3) it is well known that annealing plays an important role in eliminating defects and reducing unstable phase, thus the intrinsic n-type behavior and reduced electrical resistivity possibly turns out after annealing. Therefore, we reckon that the electrical properties of unannealed $AgBiSe_2$ may not adequately reflect the original transport behavior, while the electrical properties of annealed $AgBiSe_2$ should be close to the intrinsic properties.

To calculate the effective mass m^* of annealed $AgBiSe_2$, the carrier concentration (n) should be figured out first, because what we've got by Hall measurement system is the Hall carrier concentration (n_H). The Hall carrier concentration n_H is related to the carrier concentration n *via* $n_H = n/r_H$, where the Hall factor r_H for acoustic phonon scattering is expressed by:

$$r_H = \frac{3}{2}F_{1/2}(\eta)\frac{F_{-1/2}(\eta)}{2F_0{}^2(\eta)} \tag{1}$$

$$F_j(\eta) = \int_0^\infty \frac{x^n}{\exp(x-\eta)+1}\mathrm{d}x \tag{2}$$

where, η and F_j are the reduced Fermi energy and the j^{th} order Fermi integral, respectively. Then, assuming a single parabolic band with scattering dominated by acoustic phonons, m^* can be estimated by n and α *via* eqn (2)–(4).

$$\alpha = \frac{k_B}{e}\left[\frac{2F_1(\eta)}{F_0(\eta)} - \eta\right] \tag{3}$$

$$n = 4\pi\left(\frac{2m^*k_BT}{h^2}\right)^{3/2}F_{1/2}(\eta) \tag{4}$$

where, k_B, h and T are the Boltzmann constant, Planck constant and absolute temperature, respectively. The calculated m^* is $\sim 0.57m_0$ (m_0 is the free electron mass) for annealed $AgBiSe_2$, which is higher compared to that of $AgBiSe_2$ ($\sim 0.25m_0$) with a carrier concentration of 5.85×10^{18} cm^{-3}, and comparable to that of halogen doped $AgBiSe_2$ (~ 0.46–$0.59m_0$).[29]

The power factor of $AgBiSe_2$ and $AgSbSe_2$ is plotted in Fig. 6. Unannealed $AgSbSe_2$ exhibits the largest power factor, with a peak value of 437 μW m^{-1} K^{-2} at 590 K. However, the power factor of $AgSbSe_2$ decreases after annealing due to the

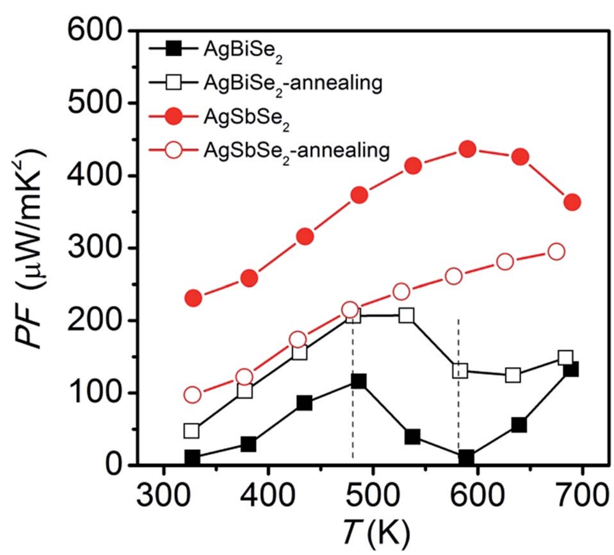

Fig. 6 Temperature dependent power factor of $AgBiSe_2$ and $AgSbSe_2$ prior to and after annealing. The two vertical dotted lines are only guides for eyes.

enhancement of electrical resistivity. Unannealed $AgBiSe_2$ and annealed $AgBiSe_2$ have the same variation trend of power factor: it increases with increasing temperature below 480 K, then decreases in the γ phase temperature range, and finally increases again above 580 K. Although the power factor of $AgBiSe_2$ increases after annealing in the entire temperature range, the maximum value 207 μW m^{-1} K^{-2} at 480 K is still relatively low.

Fig. 7 shows the thermal conductivity prior to and after annealing for $AgBiSe_2$ and $AgSbSe_2$. All samples exhibit low thermal conductivity, less than 0.7 W m^{-1} K^{-1}. Typically, the room temperature thermal conductivity values of annealed $AgBiSe_2$ and annealed $AgSbSe_2$ are 0.62 and 0.48 W m^{-1} K^{-1}, respectively. Such low thermal conductivity in I–V–VI_2 semiconductors is due to the large lattice anharmonicity arising from the lone pair electrons of Bi or Sb.[22] The thermal conductivity of $AgSbSe_2$ is even lower compared with $AgBiSe_2$, in the range of 0.44–0.48 W m^{-1} K^{-1}. The effect of annealing on the thermal conductivity of $AgBiSe_2$ and $AgSbSe_2$ is not as prominent as that on the electrical properties. The thermal conductivity of $AgBiSe_2$ is slightly reduced after annealing, and that of $AgSbSe_2$ remains substantially unchanged. Moreover, similar temperature dependence is observed in the thermal conductivity of $AgBiSe_2$, as what we have found in electrical properties previously.

The temperature dependent *ZT* values derived from the combination of the electrical and thermal transport properties are plotted in Fig. 8. $AgSbSe_2$ samples have larger *ZT* values than $AgBiSe_2$ over the entire investigated temperature range. A maximum *ZT* value of 0.60 is obtained in unannealed $AgSbSe_2$ at 640 K. However, the peak *ZT* value of annealed $AgSbSe_2$ is reduced to 0.44 at 675 K, which is mainly due to the enhancement of electrical resistivity. *ZT* value of $AgBiSe_2$ increases after annealing, especially in the temperature range of 480–640 K. Typically, the peak *ZT* value of $AgBiSe_2$ is improved from 0.18 to 0.21 after annealing.

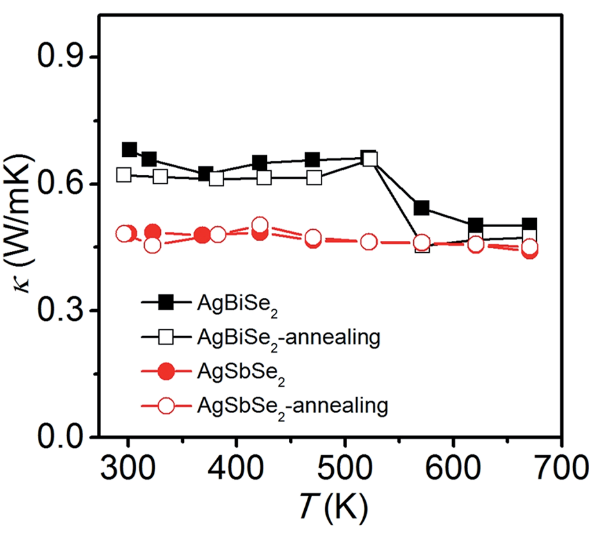

Fig. 7 Temperature dependent thermal conductivity of $AgBiSe_2$ and $AgSbSe_2$ prior to and after annealing.

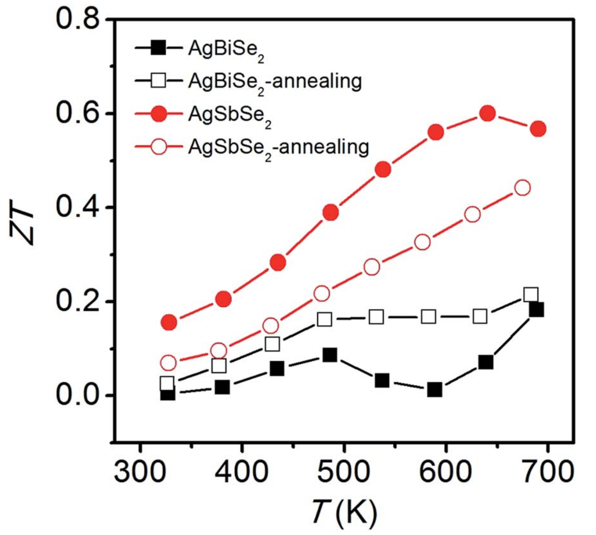

Fig. 8 Temperature dependent *ZT* of $AgBiSe_2$ and $AgSbSe_2$ prior to and after annealing.

Conclusions

In summary, $AgBiSe_2$ and $AgSbSe_2$ were synthesized by melting the mixture of elemental powders, annealing treatment was applied on the bulk samples after SPS. Annealing treatment has a great impact on thermoelectric properties of $AgBiSe_2$ due to the intriguing temperature dependent phase transition. A p–n conduction type switching is observed in unannealed $AgBiSe_2$, but electrons become the majority carrier after annealing. We reckon that the intrinsic transport behavior of $AgBiSe_2$ should be n-type, and the p-type behavior and high electrical resistivity of unannealed $AgBiSe_2$ might be caused by amount of Ag vacancies introduced *via* fabrication and the existence of mid-temperature rhombohedral phase after SPS. The peak *ZT* values are 0.18 and 0.21 for unannealed and annealed $AgBiSe_2$, respectively. $AgSbSe_2$ shows better thermoelectric performance than $AgBiSe_2$ over the entire investigated temperature range. A relatively high *ZT* value of 0.60 is achieved for unannealed $AgSbSe_2$, despite mild deterioration is observed after annealing. These findings in this work will provide an alternative way to understand the transport properties of $AgBiSe_2$ and other I–V–VI_2 compounds with phase transition. The thermoelectric performance of $AgBiSe_2$ and $AgSbSe_2$ are expected to be further enhanced by doping and/or nanostructuring.

Conflicts of interest

There are no conflicts of interest to declare.

Acknowledgements

This work was supported by the National Natural Science Foundation of China (Grant No. 51401025) and Training Program Foundation for the Beijing Municipal Excellent Talents (No. 2013D005005000004).

References

1 C. Wood, *Rep. Prog. Phys.*, 1988, **51**, 459–539.
2 G. J. Snyder and E. S. Toberer, *Nat. Mater.*, 2008, **7**, 105–114.
3 J. F. Li, W. S. Liu, L. D. Zhao and M. Zhou, *NPG Asia Mater.*, 2010, **2**, 152–158.
4 L.-D. Zhao, V. P. Dravid and M. G. Kanatzidis, *Energy Environ. Sci.*, 2014, **7**, 251–268.
5 T. Zhu, Y. Liu, C. Fu, J. P. Heremans, J. G. Snyder and X. Zhao, *Adv. Mater.*, 2017, **29**, 1605884.
6 J.-f. Li, Y. Pan, C. F. Wu, F. H. Sun and T. R. Wei, *Sci. China: Technol. Sci.*, 2017, **60**, 1347–1364.
7 J. P. Heremans, B. Wiendlocha and A. M. Chamoire, *Energy Environ. Sci.*, 2012, **5**, 5510–5530.
8 Y. Pei, H. Wang and G. J. Snyder, *Adv. Mater.*, 2012, **24**, 6125–6135.
9 J. R. Sootsman, D. Y. Chung and M. G. Kanatzidis, *Angew. Chem., Int. Ed.*, 2009, **48**, 8616–8639.
10 M. G. Kanatzidis, *Chem. Mater.*, 2010, **22**, 648–659.
11 Y. C. Lan, A. J. Minnich, G. Chen and Z. F. Ren, *Adv. Funct. Mater.*, 2010, **20**, 357–376.
12 C. Manolikas and J. Spyridelis, *Mater. Res. Bull.*, 1977, 907–913.
13 C. Xiao, X. M. Qin, J. Zhang, R. An, J. Xu, K. Li, B. X. Cao, J. L. Yang, B. J. Ye and Y. Xie, *J. Am. Chem. Soc.*, 2012, **134**, 18460–18466.
14 S. N. Guin, A. Chatterjee, D. S. Negi, R. Datta and K. Biswas, *Energy Environ. Sci.*, 2013, **6**, 2603–2608.
15 L. Pan, D. Berardan and N. Dragoe, *J. Am. Chem. Soc.*, 2013, **135**, 4914–4917.
16 X. Liu, D. Jin and X. Liang, *Appl. Phys. Lett.*, 2016, **109**, 133901.
17 F. Böcher, S. P. Culver, J. Peilstöcker, K. S. Weldert and W. G. Zeier, *Dalton Trans.*, 2017, **46**, 3906–3914.
18 H. Wang, J. F. Li, M. M. Zou and T. Sui, *Appl. Phys. Lett.*, 2008, **93**, 202106.
19 J. He, J. Xu, X. Tan, G.-Q. Liu, H. Shao, Z. Liu, H. Jiang and J. Jiang, *Journal of Materiomics*, 2016, **2**, 165–171.
20 S. Guin, S. Banerjee, D. Sanyal, S. Pati and K. Biswas, *Chem. Mater.*, 2017, **29**, 3769–3777.
21 S. Guin and K. Biswas, *Chem. Mater.*, 2013, **25**, 3225–3231.
22 D. T. Morelli, V. Jovovic and J. P. Heremans, *Phys. Rev. Lett.*, 2008, **101**, 035901.
23 M. D. Nielsen, V. Ozolins and J. P. Heremans, *Energy Environ. Sci.*, 2013, **6**, 570–578.
24 S. N. Guin, D. S. Negi, R. Datta and K. Biswas, *J. Mater. Chem. A*, 2014, **2**, 4324–4331.
25 B. A. Cook, M. J. Kramer, X. Wei, J. L. Harringa and E. M. Levin, *J. Appl. Phys.*, 2007, **101**, 053715.
26 S. H. Yang, T. J. Zhu, T. Sun, S. N. Zhang, X. B. Zhao and J. He, *Nanotechnology*, 2008, **19**, 245707.
27 J. R. Salvador, J. Yang, X. Shi, H. Wang and A. A. Wereszczak, *J. Solid State Chem.*, 2009, **182**, 2088–2095.
28 K. F. Hsu, S. Loo, F. Guo, W. Chen, J. S. Dyck, C. Uher, T. Hogan, E. K. Polychroniadis and M. G. Kanatzidis, *Science*, 2004, **303**, 818–821.
29 S. N. Guin, V. Srihari and K. Biswas, *J. Mater. Chem. A*, 2015, **3**, 648–655.
30 P. Larson and S. D. Mahanti, *Annual March Meeting*, American Physical Society, March 12–16, 2001.
31 C. Xiao, J. Xu, B. X. Cao, K. Li, M. G. Kong and Y. Xie, *J. Am. Chem. Soc.*, 2012, **134**, 7971–7977.
32 Z. Liu, J. Shuai, H. Geng, J. Mao, Y. Feng, X. Zhao, X. Meng, R. He, W. Cai and J. Sui, *ACS Appl. Mater. Interfaces*, 2015, **7**, 23047–23055.
33 S. N. Guin, A. Chatterjee and K. Biswas, *RSC Adv.*, 2014, **4**, 11811–11815.
34 S. Cai, Z. Liu, J. Sun, R. Li, W. Fei and J. Sui, *Dalton Trans.*, 2015, **44**, 1046–1051.
35 D. Li, X. Y. Qin, T. H. Zou, J. Zhang, B. J. Ren, C. J. Song, Y. F. Liu, L. Wang, H. X. Xin and J. C. Li, *J. Alloys Compd.*, 2015, **635**, 87–91.
36 M. Zhou, J. F. Li and T. Kita, *J. Am. Chem. Soc.*, 2008, **130**, 4527–4532.
37 J. Dadda, E. Müller, S. Perlt, T. Höche, P. Bauer Pereira and R. P. Hermann, *J. Mater. Res.*, 2011, **26**, 1800–1812.
38 B. H. Toby and R. B. Von Dreele, *J. Appl. Crystallogr.*, 2013, **46**, 544–549.
39 K. Hoang, S. D. Mahanti, J. R. Salvador and M. G. Kanatzidis, *Phys. Rev. Lett.*, 2007, **99**, 156403.